

Carbon Fibre Reinforced Concrete: Dependency of Bond Strength on T_g of Yarn Impregnating Polymer

Iris Kruppke^{1*}, Marko Butler², Kai Schneider², Rolf-Dieter Hund¹, Viktor Mechtcherine², Chokri Cherif¹

¹Institut für Textilmaschinen und Textile Hochleistungswerkstofftechnik, Technische Universität Dresden, Dresden, German

²Institut für Baustoffe, Technische Universität Dresden, Dresden, German

Email: *Iris.kruppke@tu-dresden.de

How to cite this paper: Kruppke, I., Butler, M., Schneider, K., Hund, R.-D., Mechtcherine, V. and Cherif, C. (2019) Carbon Fibre Reinforced Concrete: Dependency of Bond Strength on T_g of Yarn Impregnating Polymer. *Materials Sciences and Applications*, 10, 328-348.

<https://doi.org/10.4236/msa.2019.104025>

Received: November 26, 2018

Accepted: April 9, 2019

Published: April 12, 2019

Copyright © 2019 by author(s) and Scientific Research Publishing Inc.

This work is licensed under the Creative Commons Attribution International License (CC BY 4.0).

<http://creativecommons.org/licenses/by/4.0/>



Open Access

Abstract

In this paper, a method for the evaluation of the influence of different polymer suspensions and environmental conditions on adhesion between an impregnated carbon fibre heavy tow and concrete for reinforcement will be proposed. For this purpose, the impregnation material itself was investigated as a polymer film before and after incubation in water and aqueous suspensions, such as NaOH and a cementitious solution, in terms of its thermal properties, swelling behaviour and morphology. Thin polymer films were manufactured and subsequently investigated with quantification of the swelling for 28 d by thermal and scanning electron microscope analysis. The effect of pull-out shear stress was evaluated to investigate parameters such as high temperature and moisture on adhesion to concrete. Contact angle measurements were used to determine the surface energy of the polymer films. All incubated polymer films yielded a change in both surface morphology and specific residues on the polymer film surface, e.g. in the form of calcium carbonate, but no change in glass-transition temperature. A high correlation between glass-transition temperature and measured shear stress was shown during single yarn pull-out tests. Furthermore, the water treatment of pull-out samples strengthened the influence for the glass-transition temperature during the adhesion test. No influence of the surface energy of the used polymer impregnation for carbon fibres on the pull-out test was detected.

Keywords

Carbon Fibre, Concrete, Alkali Resistance, Thermo-Mechanical Resistance, Polymer Coating

1. Introduction

Textile reinforcements for concrete structures have been more and more accepted in the building industry since they offer several advantages over conventional steel reinforcement [1] [2]. A composite made of concrete and textile is typically named Textile Reinforced Concrete (TRC). This textile reinforcement consists of high-performance fibres such as alkali-resistant glass, aramid, or carbon fibres (CF). CF are not corrosive in an alkaline environment, have a high tensile strength and modulus of elasticity in the longitudinal direction of the fibre, thus they are largely suitable for use as structural reinforcement in concrete elements or for the strengthening of concrete structures [3] [4] [5]. Due to their superior mechanical and chemical properties, CF increasingly replace alkali-resistant glass fibres, which have been used in concrete for decades. Depending on the geometry of concrete elements and the loading of carbon reinforcement, CF can be shaped to rebars, biaxial grids, or multi-axial warp knitted fabrics [6].

TRC is a multi-level composite. Concrete matrix is a composite—consisting of mineral aggregates, cement particles, hydrated cement phases, water and pores. Moreover, textile reinforcement can be seen as a composite as well. At the single fibre level, each carbon filament (having a diameter of 6 μm to 7 μm) is covered by a sizing, which enables the processing of carbon fibre and defines its surface characteristics [7] [8]. At the yarn level, a bundle of a thousand single filaments is impregnated by a polymer in order to ensure load transfer from the outer filaments (which are in contact to the concrete matrix) to the majority of inner filaments of the yarn. Impregnation is inevitable since even the smallest particles in fresh concrete suspension are too large to penetrate the yarn effectively and assure sufficient inner bonding between all filaments. Consequently, TRC can be described as a multi-component system—characterised by carbon fibres, sizing, impregnation (also often called coating) and concrete. With respect to the components, different interfaces have to be taken into account. Firstly, the interface between carbon filament and sizing is an immutable factor, dependent on the supplier and manufacturing process. Secondly, the interface between sizing and coating defines the load transmission inside the filament bundle, which the textiles are made of. Thirdly, the interface between coating and inorganic cementitious matrix is responsible for the force transfer between yarn and matrix, and additionally, for the mechanical properties of the entire composite.

Due to their application in buildings, bridges and other structures and specific properties of the cementitious matrix, the CF reinforcement faces numerous challenges including heat and cold, moisture, salt, as well as a high-alkaline environment and crystallization of minerals due to cement hydration. These challenges test various properties of CF reinforcement. With regard to the bulk material, the main determining performance factors are surface functional groups, aging behaviour, thermal stability, creep behaviour, as well as strength and stiffness of carbon yarns. In terms of the textile, further factors to consider include

textile design and geometry, manufacturing process, intensity of impregnation, and degree/thickness of yarn coating due to the impregnation process. Furthermore, the following mechanisms have to be taken into account with respect to bond behaviour: chemical adhesion by covalent bonds, physical adhesion by polar forces, frictional resistance of surface against slip and surface roughness as mechanical interlock [3] [9].

By means of coating, the chemical inertness of carbon must be overcome so that a favourable adhesion to the cementitious matrix can be established. As the polymer coating is applied to the entire yarn, it tends to fill all spaces in between the filaments. Therefore, inside the yarn the polymer acts as an impregnation, which assures the load transmission from outer to inner filaments and guarantees a quasi-uniform stress and strain distribution over the yarn cross-section. It was shown in previous studies that coatings especially designed for alkali-resistant glass (AR-glass) improved the adhesion as well as the strength of these fibres in concrete [10] [11]. Besides the requirements of chemically adjusting to the sized fibre surface and of hydrating the cement-based matrix, mechanical performance, durability in an alkaline and moist environment as well as the coating temperature resistance are very important. To describe the temperature behaviour of a polymer coating, the glass-transition temperature (T_g) is an essential parameter in the context of elastic modulus and origins of the molecular structure of the polymer. For a good heat resistance and high elastic modulus, a high degree of crystallinity and high cross-linking density is needed, which can be indicated by a high T_g of polymers [12] [13]. As is known for fibre reinforced plastic rebars, the mechanical performance of polymers decrease if the temperature approaches T_g . Therefore, the load transfer into the cementitious matrix is no longer guaranteed [14]. In previous works, different types of polymers were used as matrix material for fibre rebars or for the impregnation of textile structures—both for use as reinforcement in concrete—(e.g. vinyl esters, epoxy resins, polyurethanes, polyesters, poly-(styrol-butadiene)) and as polysiloxane coatings [10] [15] [16] [17]. The T_g of thermoset resins range between 65°C and 120°C. Since poly-(styrol-butadiene), polyacrylates and polyurethanes are generated by an impregnation technique based on aqueous suspensions, their expected T_g is only roughly between -50°C and 40°C. A promising approach to increase the heat resistance of CF reinforcement for concrete is the impregnation by mineral particle suspensions, which was recently suggested by Schneider *et al.* and Nadiv *et al.* [18] [19].

Coated yarns were tested using uniaxial tension tests, by which the influence of different coatings on coherence between filaments could be assessed [20]. High-performance filaments and their interaction with different sizings were evaluated in a single-fibre tensile test [10]. However, existing testing techniques do not provide a full picture for the behaviour of the multi-component system TRC and its components under thermal and alkaline exposure as mentioned before. Initial approaches investigated the durability of sized filaments or impregnated yarns in an alkaline environment by immersion in alkaline solutions (e.g.

1 M NaOH, $pH = 14$). After exposure to elevated temperature for various time periods, the samples were extracted and tested with regard to their mechanical performance. Surface characterisation via scanning electron microscopy (SEM) helps to explain the observed mechanical behaviour. As another approach, commercially used glass fibre fabrics were tested after 28 d according to the standard of European Organisation for Technical Approvals [21]. Such an aqueous alkaline solution is composed of NaOH, KOH and $Ca(OH)_2$ to simulate the conditions in concrete during processing, curing and service life [21]. The bond performance between yarn and concrete and its durability can be assessed by pull-out tests. Butler *et al.* [22] proposed a double-sided pull-out test, whereby single yarns were embedded in concrete matrix. The samples were stored at 40°C in a fog chamber for time periods ranging from 28 d to 360 d. The measured pull-out curve was assessed in close consideration of the findings with respect to interphase morphology, which was visualised via SEM. Lorenz *et al.* [23] executed pull-out tests and tension tests on textile reinforced concrete specimens. In the pull-out tests, a short yarn segment inside the textile structure was isolated and pulled out from the surrounding concrete matrix. The test was also performed at elevated temperatures of up to 500°C . By means of tension tests on TRC plates, the complete stress-strain curve of the composite was assessed. It is the standard test method for the characterisation of the basic mechanical properties of cement-based textile-reinforced composites.

No systematic work has been published as yet on extracting and evaluating the impact of each single component of multi-component system TRC. The article at hand presents an investigation on the stability of different coatings based on aqueous suspension. For this purpose, polymer films were prepared and characterised with special respect to their swelling in various alkaline and aqueous solutions for 28 d. Additionally, thermal analysis and single-fibre pull-out tests after storage in various aqueous solutions and at different temperatures was performed to characterise the chemical and mechanical interactions of composite components under varying environmental conditions.

2. Materials and Methods

2.1. Materials

2.1.1. Coatings

Aqueous polymer dispersions were used as coating material, which differed in their chemical composition as well as in their specific thermal value (T_g). The polymers were based on acrylates (Ac1, Ac2) from CHT Beitlich GmbH (Germany), carboxylated styrol-butadienes with curing agent (SBR1), Lefasol VL90/1 [24] with Lefasol VP4-5LF [25] and without curing agent Lefasol BT83003-3 (SBR2) [26] from Lefatex Chemie GmbH (Germany), styrol-butadiene terpolymers (SBR3, SBR4) from Synthomer Deutschland GmbH (Germany) and polyurethane (PU) from Leibnitz Institute of Polymer Research Dresden (Germany).

2.1.2. Carbon Fibres

The commercially available carbon fibre Sigrafil[®] C T50-4.0/240-E100 was purchased from SGL Carbon GmbH (Germany). It has an epoxy sizing, a fineness of 3300 tex, 50 K and a single filament diameter of 7 μm .

2.1.3. Concrete

The composition of the concrete used for evaluating bond performance between impregnated carbon yarn and concrete is given in **Table 1**. The binder “Dyckerhoff NANODUR[®] compound 5941” is commercially available [27] and composed of Portland cement clinker, ground granulated blast-furnace slag and quartz powder. The aggregates were added in two portions as natural quartz sand 0/2 mm and crushed granite 2/5 mm. The workability of fresh concrete was adjusted by adding a superplasticizer to a spread of 260 mm (small cone flow table without strokes, EN 1015-3). Therefore, the concrete was suitable for casting processes. The concrete exhibited fast hardening, high compressive strength (95 MPa after 7 days, 100 MPa after 28 days), enhanced durability and moderate shrinkage (0.57 mm/m). The hardening of concrete occurred under defined climate conditions (1 day in formwork, after storage in air at 20 °C and 65% RH).

2.2. Thermal Analysis

The T_g was determined by differential scanning calorimetry (DSC) Q2000 from TA Instruments (New Castle, USA) under a nitrogen atmosphere with a heating rate of 5 K/min. The polymers were investigated as polymer films. Next to this reference, samples stored in tap water, aqueous NaOH solution as well as in alkaline solution were investigated.

2.3. Determination of Surface Energy

All investigated polymer suspensions were dried at 40 °C for 24 h followed by conditioning and curing at either 120 °C for 19 min or 150 °C for 5 min in a PTFE mold on a microscope slide. The contact angles were determined by a Drop Shape Analyzer DSA 100 (Krüss GmbH, Germany). The testing solvent were distilled water (72.8 mN/m), diiodomethane CH₂I₂ (>99%, Sigma-Aldrich Chemie GmbH, Germany, 50.8 mN/m), ethylene glycol/C₂H₆O₂ (Sigma-Aldrich Chemie GmbH, USA, 47.7 mN/m) and glycerine/C₃H₈O₃ (>98% water-free, 63.4 mN/m). At least ten individual drops were measured for each sample and solvent.

Table 1. Concrete composition based on Dyckerhoff NANODUR[®] compound 5941.

Concrete component	Mass in kg/m ³
Nanodur [®] 5914	1050
Quartz sand 0/2 mm	430
Crushed granite 2/5 mm	880
Water	168
Plasticizer	10

Calculation of the total surface energy and the polar and disperse portions was then determined according to the method developed by Owens, Wendt, Rabel and Kaelble [28] [29] [30]:

$$\frac{\gamma_l (1 + \cos \theta)}{2\sqrt{\gamma_l^d}} = \sqrt{\gamma_s^p} \left(\frac{\gamma_l^p}{\gamma_l^d} \right) + \sqrt{\gamma_s^d} \quad (1)$$

where, superscript p and d represent polar and disperse portions of the surface energies γ , while *l* and *s* represent the liquid and solid phases, *i.e.* testing solvent and polymer film surface. At least two different testing fluids should be used, which differ significantly in their polar and disperse properties.

2.4. Long-Term Stability

2.4.1. Aqueous Solution

Three different solutions were used to investigate the swelling performance of the polymer films: tap water, NaOH and filtrate of binder suspension—all as model liquids of concrete pore solution. For NaOH (Merck Chemicals GmbH, Darmstadt/Germany), a 1 M solution with *pH* of 14 was made. The cementitious solution was prepared by mixing 6.5 L water with 1 kg CEM I 42.5 R (Schwenk Zement KG, Ulm/Germany) [31] and 0.25 kg microsilica slurry from Elkem[®] 500 SE (Elkem AS in Oslo/Norway) [32]. The suspension was stored for at least 30 h without air contact and occasionally stirred. Finally, the suspension was filtered and used for durability tests [33]. The prepared cementitious solution exhibited a *pH* of 12.5. The cementitious solution shall represent the concrete pore liquid which is abbreviated from hereon as CemS.

2.4.2. Storage

To investigate long-term behaviour, disk-shaped polymer films with a diameter of 20 mm were incubated for 1 d, 3 d, 7 d, 14 d, 21 d, and 28 d in different aqueous solutions at room temperature (RT) without renewal of the medium and an initial liquid volume of 50 mL. A double determination of mass was performed and the mean value was calculated. Initial mass of the single disk-shaped polymer films was determined in the dry state and compared with the wet and swollen samples during and after storage. The samples were rinsed with distilled water and gently dried with a lint-free tissue before measuring their weight. After 28 d, all samples were dried overnight at 40°C and weighed to determine their mass degradation. These values are indicated as 29 d, dry.

2.5. Microscopic Study

All polymer films were investigated by scanning electron microscopy before and after their incubation in aqueous solution. The samples were set on a specimen holder with a carbon pad. For the investigation of the interface between the coated fibre and inorganic matrix, the tested specimens were split along the fibre direction. No further surface functionalisation for conductivity was done. A Quanta 250 FEG ESEM[™] from FEI was used at 14.00 kV and 200 Pa.

2.6. Yarn Preparation

The solid' content of the polymer dispersions was set to 30% by the addition of water. The CF yarns were impregnated by a padder bath with subsequent heating in an industrial oven including three different heating zones $\Delta\theta_1 \sim 120^\circ\text{C}$, $\Delta\theta_2 \sim 130^\circ\text{C}$ and $\Delta\theta_3 \sim 175^\circ\text{C}$ with a length of 3 m each. The process is illustrated in **Figure 1**. The process parameters of the padder bath were 1 bar contact pressure at a velocity of 2 m/min. After drying, the final coating material content of the impregnated CF was approximately 15% by mass.

2.7. Evaluation of the Bond between Yarn and Concrete

2.7.1. Setup

The bond performance of impregnated carbon yarns to the concrete matrix was characterized by means of a single-side yarn pull-out test, illustrated in **Figure 2**. The test geometry to determine the bond performance is a concrete block (dimensions: width 80 mm, depth 80 mm, height 50 mm) with a centrally positioned carbon yarn and exposed bond length of 50 mm. As an opposite bearing to the yarn, a second concrete block with a height of 90 mm was used.

During pull-out tests an increasing relative displacement s (slip) between embedded yarn and concrete along the yarns axis was measured with a relative displacement rate of 1 mm/min. The slip was recorded by two laser distance sensors positioned close to a point adjacent to the upper specimen holder, where the yarn enters the concrete block. The laser beams scanned the surface of a small aluminium clip fixed to the yarn by a small spring, which was scanned on both sides of the yarn in order to consider rotations during pull-out tests. As a result of the imposed displacement, pull-out force F is introduced into the test geometry and is counteracted at the protruding end of the carbon yarn. In order to avoid sample damage as a consequence of handling prior to testing, the lower and upper blocks were rigidly linked by a removable stainless steel frame. The frame was attached to the specimen during concrete casting and unscrewed and removed only immediately before pull-out tests. The pull-out samples were tested at different content and temperature moisture states (see **Table 2**). Since the upper concrete block featured a relatively high mass and compact geometry and thus a high thermal capacity as well as the overall duration of the pull-out test procedure being less than 5 min, the pre-conditioned samples were tested at standard lab conditions.

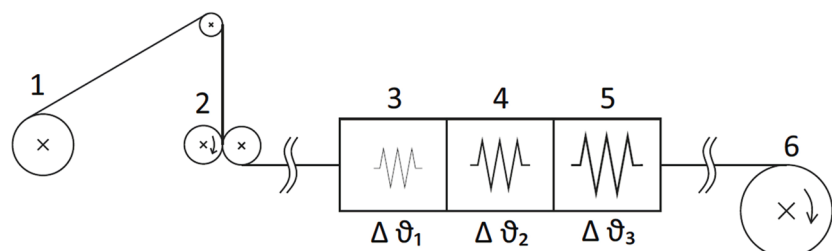


Figure 1. Coating procedure of carbon fibres, (1) CF bobbin, (2) bath coating via padder, (3)-(5) heating zones $\Delta\theta_1$, $\Delta\theta_2$ and $\Delta\theta_3$, and (6) wind-up onto aluminium coil.

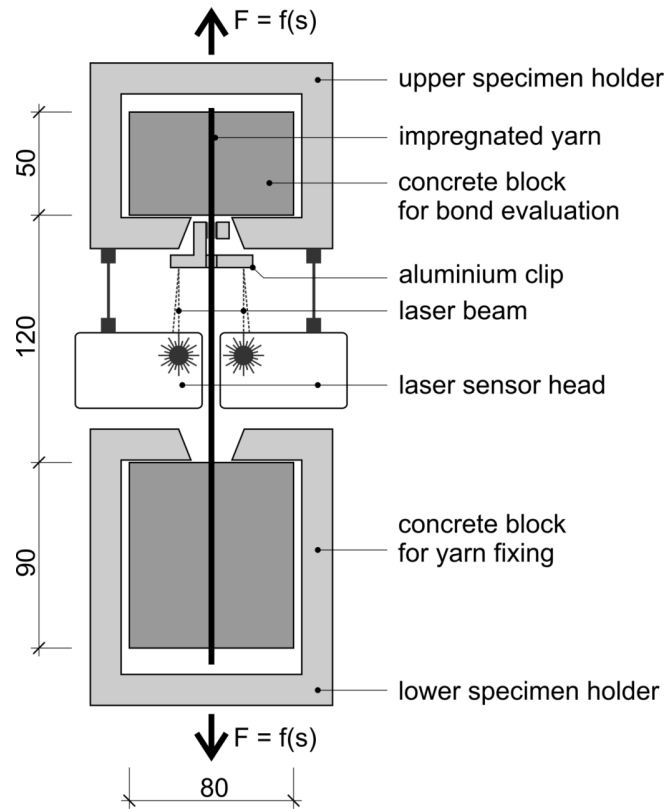


Figure 2. Schematic representation of the pull out test.

Table 2. Conditions for sample curing pull-out tests, day 7 measurements.

Test conditions during pull-out test	Environmental conditions at concrete age of	Environmental conditions at concrete age of
	1 d to 6 d	1 d to 6 d
Dry, -20°C	In freezer at -20	Freezing to -20°C
Dry, 20°C	In air at 20°C , 65% RH	
Dry, 95°C	In air at 20°C 65% RH	Heating to 95°C , no moisture control
Wet, -20°C	In water at 20°C	Freezing to -20°C
Wet, 20°C	In water at 20°C	
Wet, 95°C	In water at 20°C	Heating to 95°C , no moisture control

2.7.2. Sample Production and Curing

The pull-out specimens were produced by casting. Before casting fresh concrete into the moulds for the upper and lower concrete block, the impregnated carbon yarn was placed centrally and stretched in the form work. For this purpose, the yarn was threaded through openings in the front sides of both moulds and fixed by rubber fittings. After complete filling of the form works, the removable stainless steel frame, in particular its fixing to the concrete, was embedded into the blocks surface.

After casting, the concrete surface was sealed under a plastic foil. The specimens were demoulded after one day and stored at various conditions for six

more days until testing (see **Table 2**).

2.7.3. Analysis of Results

During pull-out tests, vs. force displacement curves were recorded. In order to exclude the effect of differing yarn circumferences (and therefore, of varying the bonding surfaces) on results, the measured force and displacement were transformed to shear stress vs. slip curves. Since the majority of tested yarns featured flat, elliptical cross-sections (with varying radii of their semiaxis) the dimensions of yarns were determined at the upper and lower sides of the test block. Thus, a hypothetical circumference u of a corresponding ellipse was calculated. The diameter or the shape of the yarn cross-section has to be chosen carefully due to the resulting contact area for further calculations. The shear stress τ was obtained by division of the pull-out force F by the contact area yielding from the hypothetical circumference, times the embedment length l of the yarn (Equation (2)).

$$\tau = \frac{F}{u \cdot l} \quad (2)$$

For each curve, five discretionary values were determined in order to characterise the pull-out behaviour of the different yarn coatings (see **Figure 3**):

- Maximum shear stress: τ_{\max}
- Shear stress at slip of 0.5 mm: $\tau_{0.5}$ mm
- Shear stress at slip of 1.0 mm: $\tau_{1.0}$ mm
- Specific pull out work at slip of 0.5 mm: $W_{0.5}$
- Bond modulus as secant to the curve between $\tau_{0.2} = 0.2 \tau_{\max}$ and $\tau_{0.7} = 0.7 \tau_{\max}$

2.8. Statistics

All measurements were performed at least in triplicate, except for T_g measurements, which were in duplicate. The values are provided as mean \pm standard deviation. Two-way analysis of variance (ANOVA) with a Tukey correction

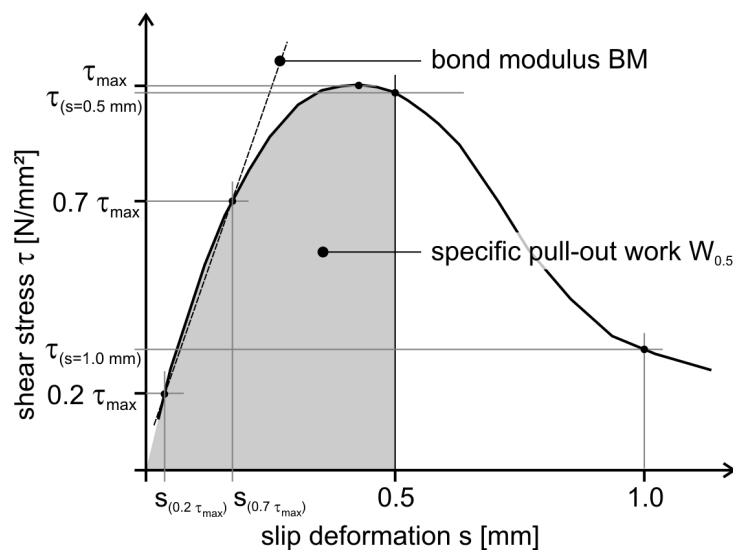


Figure 3. Scheme of stress-slip curve obtained from yarn pull-out tests.

comparison single-step procedure was applied for statistical evaluation, and p values > 0.05 were considered significant; they are indicated by an asterisk (*).

3. Results and Discussion

3.1. Polymer

The determined glass-transition temperature (T_g) for dried specimen was not affected by the applied conditions in different aqueous and alkaline solutions (Table 3). The determination of T_g was performed at least by two heating cycles (HC).

All polymers differ in their polar and total surface energy, due to their chemical composition, while their disperse surface energies are quite comparable, being in the range of 23 mN/m to 35 mN/m (see Table 4). The highest polar surface energy was measured for SBR3, with 29 mN/m, followed by acrylate (Ac1) at 22.0 mN/m, and poly-urethane (PU) with 21.6 mN/m. These polymers also exhibited the highest total surface energy. For these coatings, the contact angles of water were <45°. The least polar surface energy was observed for Ac2 and SBR1, which exhibited the highest water contact angles with more than 70°. Nevertheless, all polymers can be classified as hydrophobic.

Table 3. T_g of all polymers under investigation determined by DSC of polymer films by multiple heating cycles (HC).

	T_g (5th HC)	T_g [Water] (2nd HC)	T_g [NaOH] (2nd HC)	T_g [CemS] (2nd HC)
	°C	°C	°C	°C
SBR1	-8	-9	-8	-8
SBR2	-5	-5	-3	-5
SBR3	-5	-5	-5	-6
SBR4	33	32	33	29
Ac1	13	13	12	13
Ac2	39	41	38	44
PU	no T_g between -30°C and 100°C			

Table 4. Contact angles (CA) and polar and disperse parts of surface energy γ of the polymer films made of Ac1, Ac2, PU, SBR1, SBR2, SBR3 and SBR4.

	Ac1	Ac2	PU	SBR1	SBR2	SBR3	SBR4
CA H ₂ O in °	44.2 ± 3.0	72.5 ± 2.7	37.0 ± 3.7	79.0 ± 4.7	53.3 ± 4.4	29.8 ± 2.6	55.9 ± 1.0
CA CH ₂ I ₂ in °	45.0 ± 1.4	50.3 ± 1.7	28.0 ± 2.1	42.7 ± 6.7	50.0 ± 2.4	42.7 ± 2.6	49.6 ± 3.3
CA C ₂ H ₅ O ₂ in °	43.5 ± 1.0	67.4 ± 1.0	44.9 ± 2.6	47.7 ± 3.7	39.8 ± 3.5	22.8 ± 4.8	40.2 ± 2.1
CA C ₃ H ₈ O ₃ in °	64.2 ± 2.1	84.1 ± 2.0	73.3 ± 0.6	65.6 ± 5.5	73.2 ± 3.2	41.2 ± 5.6	59.3 ± 0.8
γ_{polar} in mN/m	22.1	7.5	21.6	4.1	17.6	29.7	16.6
$\gamma_{disperse}$ in mN/m	24.3	22.9	25.8	35.2	23.8	28.0	27.0
γ_{total} in mN/m	46.4	30.4	47.4	39.3	41.4	57.7	43.6

3.2. Long-Term Stability

The long-term stability of the polymer was investigated by placing polymer film samples in three different aqueous solutions. The mass increased over the storage duration of 28 d for all conditions as in the case of static placement in water (Figure 4), NaOH (Figure 5), and cementitious solution (Figure 6). Surface topography was characterised by SEM-imaging, before and after incubation (Figure 7). All polymer films initially exhibited a smooth and clean surface, which is shown as an example for SBR3 in Figure 7(A). Generally, two different tendencies can be described: a pronounced increase in mass over the 28 days and a nearly constant mass level. This could be observed for all aqueous solutions.

For the exposure to water, swelling of the polymer film was determined by continuous increase in mass for SBR1. For the other polymers, the swelling level did not change significantly in comparison to the state attained during the first day of placement in water. This indicates an equilibrium between the elastic portions of the polymer network (restoring forces) and water (osmotic pressure), which diffuses into the rubber gaps of the investigated polymers [34] [35]. After incubation and drying (day 29, dry), a decrease in mass compared to the initial weight was observed for all samples (see Table 5). This mass loss does not seem to be related to the previous swelling procedure. SBR2 exhibits the highest decrease in mass with 11.5%, compared to its initial mass, which was not expected when taking into account its inconspicuous swelling behaviour. Ac1 and SBR4 demonstrate the lowest loss in mass after incubation in water. The detected losses in mass can be explained by washing out components of the polymer films, such as plasticisers. Furthermore, the subsequent SEM investigation did not show any significant changes in surface morphology of the polymer films. A reference material (SBR3 was used as an example) does not show initial precipitates

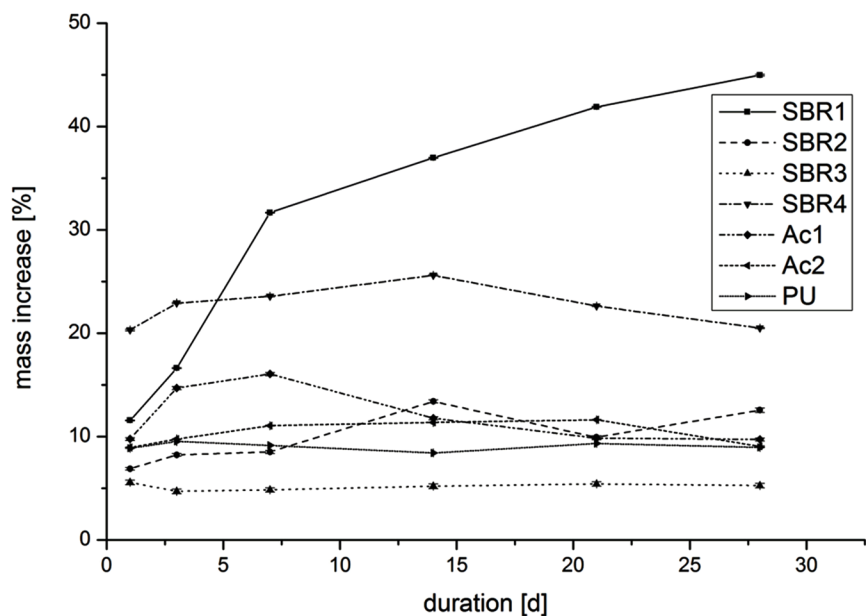


Figure 4. Mass increase resulting from the incubation of polymers in water.

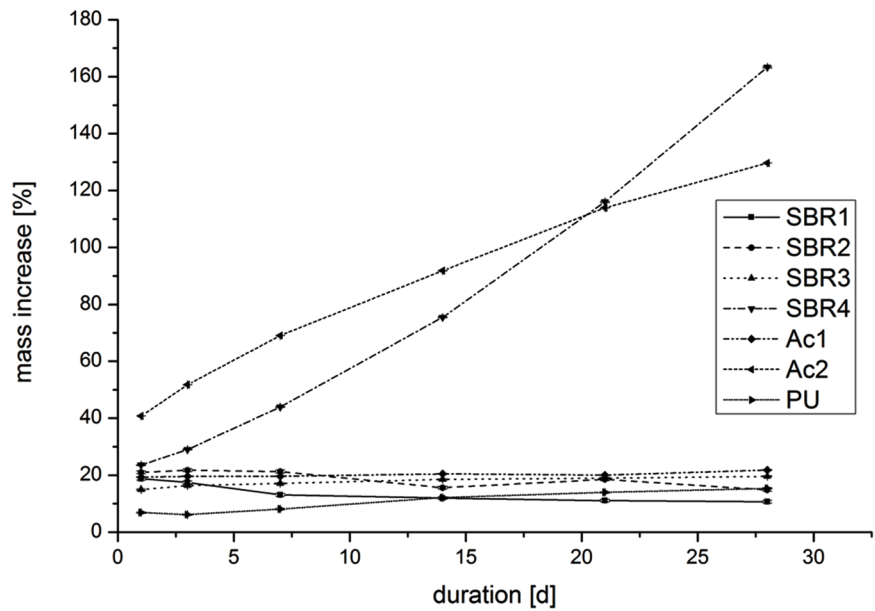


Figure 5. Mass increase resulting from the incubation of polymers in aqueous NaOH.

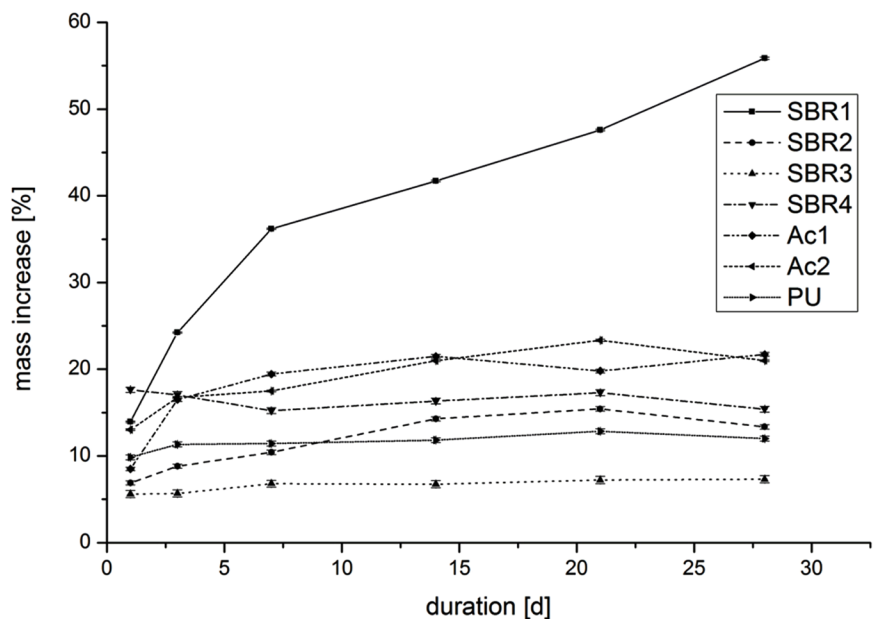


Figure 6. Mass increase resulting from the incubation of polymers in cementitious aqueous solution.

on its surface (**Figure 7(A)**), but may exhibit some roughening after incubation (this is the case for SBR2, SBR3, PU, Ac1) and dehydration cracks (SBR1, SBR4). Corresponding images are not shown.

For incubation in NaOH, the results are shown in **Figure 5**. Here, SBR4 as well as Ac2 exhibit a steady swelling over 28 days, while all other polymer films reach a constant mass increase of less than 20%. The increase in mass by 163% for SBR4 and 130% for Ac2 represents a combination of water absorption and precipitation of NaOH. Later ones (29 d) are identified by their increase in mass

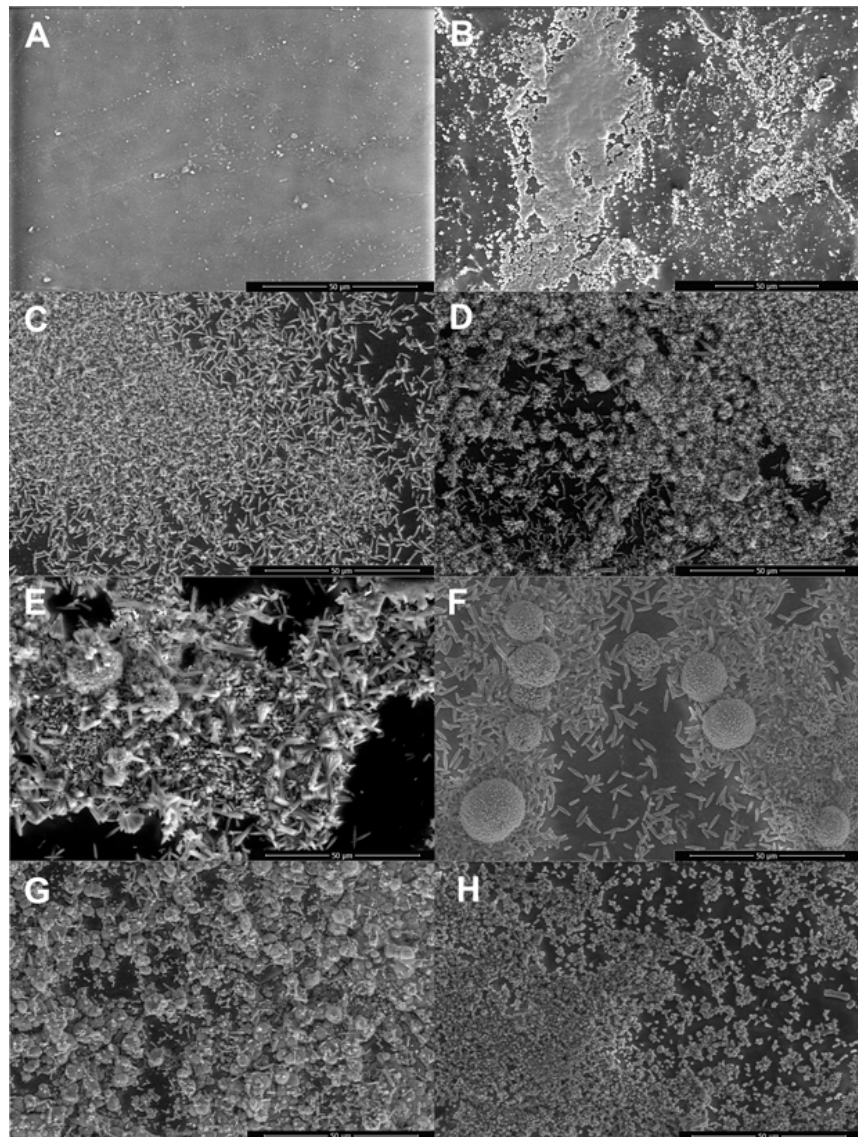


Figure 7. Scanning electron micrographs of polymer films after static incubation in the cement solution; (A) reference for SBR3 and polymer films after incubation: (B) Ac1, (C) Ac2, (D) PU, (E) SBR1, (F) SBR2, (G) SBR3, and (H) SBR4.

Table 5. Changes in polymer mass due to incubation for 28 d and drying at 29 d.

	Water	NaOH	CemS
	[%]	[%]	[%]
SBR1	-2.1	-2.8	1.9
SBR2	-11.5	-5.8	2.7
SBR3	-2.0	-1.8	-0.8
SBR4	-0.7	6.4	2.4
Ac1	-0.4	-0.8	3.6
Ac2	-1.1	4.0	3.0
PU	-2.2	-2.6	-0.3

after drying (29 d, dry) compared to the original state, supplemented via SEM investigations (images are not shown in this article). For both polymer films, a complete covering with crystalline precipitates was observed. These NaOH crystallite stacks exhibited a length around 20 - 25 μm and a width of approximately 10 μm for SBR4 and Ac2. In contrast to this, SBR1 showed smaller crystalline, finely dispersed, needle-shaped NaOH structures (in the range of $4.8 \pm 0.8 \mu\text{m}$ and thickness of 0.3 μm up to 0.7 μm) comparable to those shown in the literature [36] [37]. Interestingly, NaOH crystals also developed inside of dehydration cracks of the polymer film of SBR1, without causing a measurable increase in mass when measured after drying (Table 5). The other polymer films did not show any changes in surface morphology and had a smooth surface apart from some dehydration cracks.

Incubation in the cementitious solution yielded a considerable initial increase in mass by 5% to 20% in the wet state for all polymer films except SBR1 (Figure 6). Only for the acrylates, Ac1 and Ac2, there was a comparably small increase over 28 days. Also, SBR3 with 7.3% and PU with 12.0% exhibited the lowest final level of increase. These two polymer films got washed out, which resulted in a final decrease in mass after drying of -0.8% for SBR3, and -0.3% for PU. The other polymer films exhibited an increase in mass after incubation in the cementitious solution and subsequent drying of between 1.9% for SBR1 and 3.6% for Ac1 (Table 5).

Additionally, incubation in the cementitious solution caused the most recognisable changes in surface morphology as visualised by SEM (Figures 7(B)-(H)). Different types of characteristic calcium silicate hydrate phases are visible: For the polymer films with the highest increase in mass over time (SBR1, Ac1, Ac2), a dense layer of crystals can be seen. Depending on the surface functionality and the swelling behaviour in the solution, the precipitated crystals differ in size and shape. The mineral on SBR1, which formed an almost closed surface layer, is presumably calcite (Figure 7(E)). The observed dumbbell-shaped crystals are comparable to those reported in the literature [38] [39]. In comparison to the other polymer films, the degree of coverage is comparatively low. Caused by the swelling, the SBR1 polymer film exhibits a high number of dehydration cracks. The surface of PU films, incubated in the cementitious solution, is characterised by crystals of two different shapes. There are dumbbell-shaped crystals of different sizes built from needle-like crystals and spherulitic sponge-like crystals (Figure 7(H)). Compared to this, no dumbbell-shaped formations could be observed for Ac2. Instead, only needle-shaped and various elongated calcite crystals were found (Figure 7(C)). According to its low surface energy (Table 4), the low coverage by precipitates of the Ac2 polymer film led to the assumption of a low association of crystals to the surface. Only for SBR4 are there additional fine crystalline particles besides calcite (bottom crystals, needles, dumbbells), such as portlandite with its hexagonally shaped crystals [40], shown in Figure 7(D).

From the presented results, it can be concluded that swelling of the polymers causes an initial increase in mass between 5% and 25%. The swelling degree does

not show correlation to the polymers' contact angle to water and even high ionic strength liquids (NaOH, cementitious solution) do not significantly alter the swelling properties. In addition to swelling, the observed increase in mass is caused by mineral precipitates, which again do not relate to the polymer film surface chemistry nor to the surrounding liquids. Those mineral precipitates may influence the bonding interface between CF coating and concrete.

3.3. Evaluation of Yarn-Concrete Bond

Figure 8 describes the distinct dependence of the maximum shear stress τ_{\max} and the applied conditions for sample curing and testing (see **Table 2**). Depending on the temperature and the humidity of concrete curing, two trends are visible. Firstly, with increasing temperature, the maximum shear stress decreases significantly. Secondly, with increasing humidity, the impact of temperature on maximum shear stress is markedly increased. A comparable trend was also observed for shear stress at a slip deformation of 1.0 mm $\tau_{1.0}$ mm (data not shown).

The climate conditions during concrete curing and sample testing are a strengthening influence on bond behaviour of the chemistry of CF coating and its T_g , since only few significant differences between the coatings have been identified. The influence of temperature will be discussed as a function of the present T_g of the coatings under investigation. As presented in **Table 3**, the coatings SBR4 and Ac2 exhibit the highest T_g of 32°C and 39°C, respectively. The other coatings show lower T_g values which let expect a lower mechanical resistance by these polymers, as they already passed out of the glassily condition.

For SBR4 and Ac2, the T_g is not reached at room temperature, thus they do show the highest maximum pull out force at +20°C and 65% relative humidity (**Figure 8**). Below the T_g , the mechanical properties of a polymer can be seen as

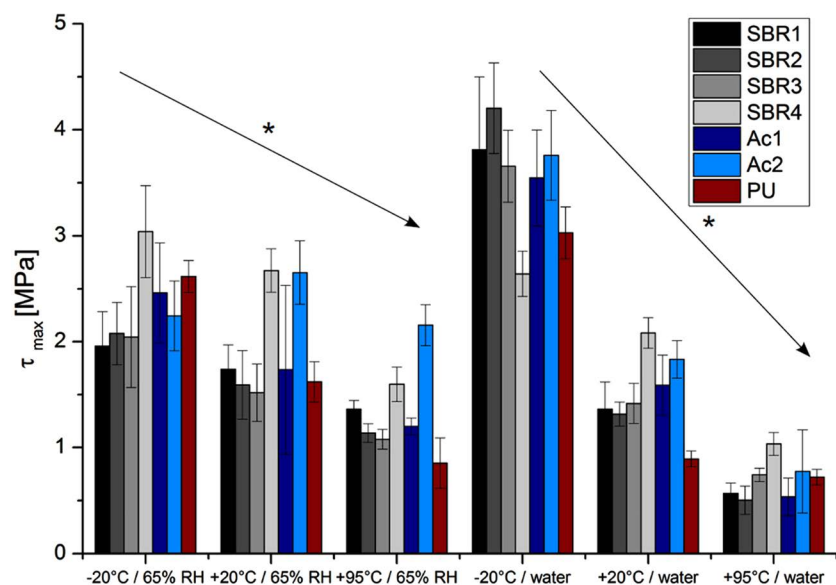


Figure 8. Shear strength τ_{\max} for various climatic conditions, such as 65% relative humidity (RH) and submersion in water; standard deviations are given.

constant. Therefore, for the coatings SBR4 and Ac2 with high T_g ($>20^\circ\text{C}$), the τ_{\max} is on the same level for both $+20^\circ\text{C}$ and -20°C at 65% relative humidity. In comparison to this and caused by its relatively high T_g of 33°C , SBR4 continues to exhibit a good performance in the pull-out testing of wet samples at room temperature. However, τ_{\max} decreases by 78% in comparison to the specimens stored in the standard lab environment ($+20^\circ\text{C}$, 65% RH). This could be explained by intense swelling of SBR4 in water caused by the destabilisation of the polymer network through water. The maximum shear stress of Ac2 decreased to 69% of the initial value as a result of the composite incubation in water. For this polymer as well, a high increase in mass of the film in NaOH was observed due to crystal formation on the polymer coating. For the room temperature with water storage and storage at 65% relative humidity, the lowest change of the maximum shear stress could be observed for SBR3 which exhibits the lowest increase in mass or swelling over 28 days in all incubation media (water, NaOH as well as cementitious solution). For various polymer systems, a relationship between the decrease in the glass transition temperature and the increase in humidity as well as swelling was found [41] [42]. With respect to the mechanical performance of the coating polymers after incubation in water, a reduction of τ_{\max} was observed and obviously driven by the T_g and affected by polymer swelling.

In contrast to the specimens stored at 65% RH, the maximum shear stress decreases pronouncedly as a result of incubation in hot water (95°C with water incubation). These effects are clearly driven by the presence of water and its aggregate states. Therefore, for the water incubated samples, a freeze effect at -20°C can be reasonably assumed due to the ice crystal formation of free water in the composite. The ice crystals were also formed in the interphase between concrete and impregnated yarn which intensified the bond between these components. Thus, a reinforcing effect is provided on the interfaces of multi-component systems, whereas the τ_{\max} was at least doubled, except for SBR4 with an increase of only 27%. For the associated pull-out work at $-20^\circ\text{C}/\text{wet}$, a significant effect of ice formation was recognised. It can be assumed that the ice crystal formation increases the rigidity and reduces the (fracture) toughness of yarn-concrete interphase. Thus, a more brittle/less viscous failure of bond mechanisms during pull-out occurs, accompanied by higher maximum shear stresses (see **Figure 8**).

For the determined bond modulus and therefore to describe the elastic properties of the composite, neither an influence of the T_g of the polymers nor of the polar surface energy could be inferred. To further characterise the bond behaviour, the specific pull-out work at slip deformation of 0.5 mm $W_{0.5}$ between coated carbon yarn and concrete was calculated. At 95°C , the values reached a minimum for both types of submersion, *i.e.* at 65% relative humidity and in water. It can be assumed that at this temperature, since T_g is passed, a viscous slip deformation of polymer molecules occurs between carbon fibre and concrete. The described, significant effect could be especially observed for all polymers (Ac1, SBR2, SBR3, and PU), whose T_g was already exceeded at room tempera-

ture conditions. In this case, a decreased specific pull-out work was calculated at +20°C/65% RH (data not shown). Thus, as Ac2 exhibits a high T_g but a low polar surface energy (Table 4), it can be assumed that a high influence of the T_g onto the specific pull-out work exists. This is consistent with the comparably high pull-out work of SBR4 at +20°C/65% RH, which has the second highest T_g . Here, a good impregnation by the coating as well as a good association of inorganic matrix onto the impregnated yarn could be observed. SBR4 serves as an example (Figure 9).

Furthermore, it has to be taken in account that a constant swelling of a polymer causes a reduction of water in the interface region between yarn coating and surrounding inorganic matrix material which is present during the hardening process of the concrete. Here, a lack of water is potentially weakening this interface by less hardened concrete, resulting in a decrease of the maximum shear stress, as shown for SBR1, SBR2 and SBR3. In this case, the glass-transition temperature is already passed and only the swelling effects have to be considered for the bond strength.

4. Conclusion

After incubation in water or water-based alkaline solutions, the glass-transition temperature of polymers under investigation does not change. Polymers which exhibit a contact angle for water < 45°C show a high polar surface energy. After one week of incubation in aqueous solutions, most of the investigated systems reached an equilibrium state of mass increase. For some polymers, however, a further swelling in different solutions was observed, which concurs with residues or crystal growth verified via SEM images. A distinct relationship between the maximum shear stress measured in the yarn pull-out test and the glass-transition temperature and its swelling could be observed. The higher the glass-transition

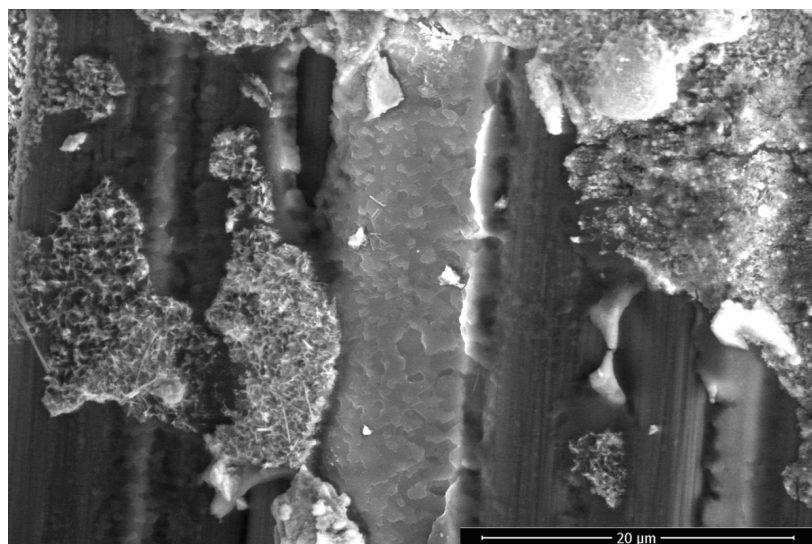


Figure 9. Scanning electron microscope image of a pull-out test specimen: pulled out SBR4 coated CF yarn with residues of inorganic matrix.

temperature, the higher the bond strength between the investigated polymer coated yarn and concrete matrix that gets reduced by high humidity. Another highly relevant parameter is the specific pull-out work, which together with the obtained complete force-slip curve, makes the single fibre pull-out test a key tool to examine the quality of polymer coatings of carbon yarns with respect to their bond to the concrete matrix in textile reinforced concrete. Based on the results of this study, the thermo-mechanical characteristics are more important than ever for the carbon fibre reinforced concrete. Therefore, pursuing studies will be done in the field of thermo-mechanical properties of coatings on yarns as well as in the field of high-temperature resistant coatings.

Acknowledgements

The Federal Ministry of Education and Research by C³—Carbon Concrete Composite BMBF, 03ZZ0302A is gratefully acknowledged.

Conflicts of Interest

The authors declare no conflicts of interest regarding the publication of this paper.

References

- [1] Mechtcherine, V. (2013) Novel Cement-Based Composites for the Strengthening and Repair of Concrete Structures. *Construction and Building Materials*, **41**, 365-373. <https://doi.org/10.1016/j.conbuildmat.2012.11.117>
- [2] Brameshuber, W. (2006) Report rep036: Textile Reinforced Concrete State-of-the-Art Report of RILEM TC 201-TRC. Springer, Berlin.
- [3] Busel, J.P. and Shield, C.K. (2006) Guide for the Design and Construction of Structural Reinforced with FRP Bars. ACI Committee 440.
- [4] Dvorkin, D. and Peled, A. (2016) Effect of Reinforcement with Carbon Fabrics Impregnated with Nanoparticles on the Tensile Behavior of Cement-Based Composites. *Cement and Concrete Composites*, **85**, 28-38. <https://doi.org/10.1016/j.cemconres.2016.03.008>
- [5] Lee, C., Bonacci, J.F., Thomas, M.D.A., Maalej, M., Khajepour, S., Hearn, N., Pantazopoulou, S. and Sheikh, S. (2000) Accelerated Corrosion and Repair of Reinforced Concrete Columns Using Carbon Fibre Reinforced Polymer Sheets. *Canadian Journal of Civil Engineering*, **27**, 941-948. <https://doi.org/10.1139/l00-030>
- [6] Hausding, J., Engler, T., Kleicke, R. and Cherif, C. (2008) High Productivity and Near-Net Shape Manufacture of Textile Reinforcements for Concrete.
- [7] Dai, Z., Shi, F., Zhang, B., Li, M. and Zhang, Z. (2011) Effect of Sizing on Carbon Fiber Surface Properties and Fibers/Epoxy Interfacial Adhesion. *Applied Surface Science*, **257**, 6980-6985. <https://doi.org/10.1016/j.apsusc.2011.03.047>
- [8] Tang, L.-G. and Kardos, J.L. (1997) A Review of Methods for Improving the Interfacial Adhesion between Carbon Fiber and Polymer Matrix. *Polymer Composites*, **18**, 100-113. <https://doi.org/10.1002/pc.10265>
- [9] K ppler, I., Matth i, P. and Cherif, C. (2014) Adhesion Problematic for Novel Non-Crimp Fabric and Surface Modification of Carbon-Fibres Using Oxy-Fluorination. *International Journal of Chemical, Nuclear, Materials and Metallurgical Engineer-*

- ing, **8**, 1390-1395.
- [10] Scheffler, C., Gao, S.L., Plonka, R., Mäder, E., Hempel, S., Butler, M. and Mechtcherine, V. (2009) Interphase Modification of Alkali-Resistant Glass Fibres and Carbon Fibres for Textile Reinforced Concrete I: Fibre Properties and Durability. *Composite Science and Technology*, **69**, 531-538.
<https://doi.org/10.1016/j.compscitech.2008.11.027>
- [11] Scheffler, C., Gao, S.L., Plonka, R., Mäder, E., Hempel, S., Butler, M. and Mechtcherine, V. (2009) Interphase Modification of Alkali-Resistant Glass Fibres and Carbon Fibres for Textile Reinforced Concrete II: Water Adsorption and Composite Interphases. *Composite Science and Technology*, **69**, 905-912.
<https://doi.org/10.1016/j.compscitech.2008.12.020>
- [12] Apicella, A., Nicolais, L., Astarita, G. and Drioli, E. (1979) Effect of Thermal History on Water Sorption, Elastic Properties and Glass Transition Temperature of Epoxy Resins. *Polymer*, **20**, 1143-1148. [https://doi.org/10.1016/0032-3861\(79\)90307-0](https://doi.org/10.1016/0032-3861(79)90307-0)
- [13] Boogh, L. and Manson, J.-A.E. (1999) Dendritic Hyperbranched Polymers as Tougheners for Epoxy Resins. *Polymer*, **40**, 2249-2261.
[https://doi.org/10.1016/S0032-3861\(98\)00464-9](https://doi.org/10.1016/S0032-3861(98)00464-9)
- [14] Katz, A., Berman, N. and Bank, L.C. (1999) Effect of High Temperature on Bond Strength of FRP Rebars. *Journal of Composites for Construction*, **3**, 73-81.
[https://doi.org/10.1061/\(ASCE\)1090-0268\(1999\)3:2\(73\)](https://doi.org/10.1061/(ASCE)1090-0268(1999)3:2(73))
- [15] Alsayed, S., Al-Salloum, Y., Almusallam, T., El-Gamal, S. and Aqel, M. (2012) Performance of Glass Fiber Reinforced Polymer Bars under Elevated Temperatures. *Composites. Part B*, **43**, 2265-2271.
<https://doi.org/10.1016/j.compositesb.2012.01.034>
- [16] Kruppke, I., Hund, R.-D. and Cherif, C. (2015) Adhesion Problematics and Curing Kinetics in a Thermosetting Matrix for Stitch-Free Non-Crimp Fabric. *Textile Research Journal*, 1-12.
- [17] Shayed, M.A., Hund, H., Hund, R.-D. and Cherif, C. (2016) Thermal and Oxidation Protection of Carbon Fiber by Continuous Liquid Phase Pre-Ceramic Coatings for High Temperature Application. *Fibers and Polymers*, **17**, 229-240.
<https://doi.org/10.1007/s12221-016-5689-3>
- [18] Peled, C.R., Mechtcherine, A., Hempel, V. and Schroefl Nadiv, S. (2017) Micro- and Nanoparticle Mineral Coating for Enhanced Properties of Carbon Multifilament Yarn Cement-Based Composites. *Composites Part B*, **111**, 179-189.
<https://doi.org/10.1016/j.compositesb.2016.12.005>
- [19] Schneider, K., Lieboldt, M., Liebscher, M., Fröhlich, M., Hempel, S., Butler, M., Schröfl, C. and Mechtcherine, V. (2017) Mineral-Based Coating of Plasma-Treated Carbon Fibre Rovings for Carbon Concrete Composites with Enhanced Mechanical Performance. *Materials*, **10**, 1-17. <https://doi.org/10.3390/ma10040360>
- [20] Textile Glass-Yarns Determination of Breaking Force and Breaking Elongation, ISO 3341:2000-05, DIN Deutsches Institut für Normung e. V., 2000.
- [21] E.O. for T.A. Europäische Organisation für Technische Zulassungen (2001) Bekanntmachung der Leitlinie für Aussenseitige Wärmedämm-Verbundsysteme, Eidgenössisches Finanzdepartement EFD, Bundesamt für Bauten und Logistik BBL.
- [22] Butler, M., Mechtcherine, V. and Hempel, S. (2009) Experimental Investigations on the Durability of Fibre-Matrix Interfaces in Textile-Reinforced Concrete. *Cement & Concrete Composites*, **31**, 221-231.
<https://doi.org/10.1016/j.cemconcomp.2009.02.005>
- [23] Lorenz, E., Schütze, E., Schladitz, F. and Curbach, M. (2013) Textilbeton Grundle-

- gende Untersuchungen im Überblick. *Beton- und Stahlbetonbau*, **108**, 711-722.
<https://doi.org/10.1002/best.201300041>
- [24] L.C. GmbH (2014) Lefasol VL 90/1.
- [25] L.C. GmbH (2013) Lefasol VP 4-5 LF.
- [26] L.C. GmbH (2015) Lefasol BT 83003-3.
- [27] D. GmbH (2017) Dyckerhoff NANODUR® Compound 5941, zur einfachen Herstellung von UHPC.
- [28] Kaelble, D.H. and Uy, K.C. (1970) A Reinterpretation of Organic Liquid-Polytetrafluoroethylene Surface Interactions. *The Journal of Adhesion*, **2**, 50-60.
<https://doi.org/10.1080/0021846708544579>
- [29] Owens, D.K. and Wendt, R.C. (1969) Estimation of the Surface Free Energy of Polymers. *Journal of Applied Polymer Science*, **13**, 1741-1747.
<https://doi.org/10.1002/app.1969.070130815>
- [30] Rabel, W. (1977) Liquid Interfaces in Theory and Applied Technology. *Physikalische Blätter*, **33**, 151-156. <https://doi.org/10.1002/phbl.19770330402>
- [31] S.Z. KG (2012) Technisches Merkblatt, CEM I 42,5 R, Portlandzement. Schwenk Zement KG.
- [32] E.M. Inc. (2013) Safty Data Sheet, Elkem Microsilika Textsuperscript®. Elkem Materials Inc.
- [33] Butler, M. (2009) Dauerhaftigkeit von Verbundwerkstoffen aus Zementgebundenen Martices und AR-Glas-Multifilamentgarnen. Schriftenreihe des Institutes für Baustoffe Heft 2009/1.
- [34] Candau, S., Bastide, J. and Delsanti, M. (2005) Structural, Elastic, and Dynamic Properties of Swollen Polymer Networks. *Advances in Polymer Science*, **48**, 27-71.
- [35] Mostafa, A., Abouel-Kasem, A., Bayoumi, M.R. and El-Sebaie, M.G. (2009) Effect of Carbon Black Loading on the Swelling and Compression Set Behavior of SBR and NBR Rubber Compounds. *Materials and Design*, **30**, 1561-1568.
<https://doi.org/10.1016/j.matdes.2008.07.043>
- [36] Mootz, D. and Seidel, R. (1990) Zum System Natriumhydroxid—Wasser Die Kristallstruktur der metastabilen Phase Beta-NaOH·4H₂O. *Journal of Inorganic and General Chemistry*, **582**, 162-168.
- [37] Stehr, H. (1967) Neubestimmung der Kristallstrukturen des dimorphen Natriumhydroxids, NaOH, bei verschiedenen Temperaturen mit Röntgenstrahl und Neutronenbeugung. *Zeitschrift für Kristallographie Crystalline Materials*, **125**, 332-359.
<https://doi.org/10.1524/zkri.1967.125.125.332>
- [38] Buczynski, C. and Chafetz, H.S. (1990) Habit of Bacterially Induced Precipitates of Calcium Carbon and the Influence of Medium Viscosity on Mineralogy. *Journal of Sedimentary Petrology*, **61**, 226-233.
<https://doi.org/10.1306/D42676DB-2B26-11D7-8648000102C1865D>
- [39] Meldrum, F.A. and Hyde, S.T. (2001) Morphological Influence of Magnesium and Organic Additives on the Precipitation of Calcite. *Journal of Crystal Growth*, **231**, 544-558. [https://doi.org/10.1016/S0022-0248\(01\)01519-6](https://doi.org/10.1016/S0022-0248(01)01519-6)
- [40] Kumar, S., Kumar, R., et al. (2008) Mechanical Activation of Granulated Blast Furnace Slag and Its Effect on the Properties and Structure of Portland Slag Cement. *Cement & Concrete Composites*, **30**, 679-685.
<https://doi.org/10.1016/j.cemconcomp.2008.05.005>

- [41] Kelley, F.N. and Bueche, F. (1961) Viscosity and Glass Transition Relations for Polymer-Diluent Systems. *Journal of Polymer Science*, **50**, 549-556. <https://doi.org/10.1002/pol.1961.1205015421>
- [42] Mackague, E.L., Reynolds, J.D. and Halkias, J.E. (1978) Swelling and Glass Transition Relations for Epoxy Matrix Material in Humid Environments. *Journal of Applied Polymer Science*, **22**, 1643-1654. <https://doi.org/10.1002/app.1978.070220615>